Marine Chemistry 125 (2011) 26–38

Contents lists available at ScienceDirect

Marine Chemistry

journal homepage: www.elsevier.com/locate/marchem

Fluorescence: Absorption coefficient ratio — Tracing photochemical and microbial degradation processes affecting coloured dissolved organic matter in a coastal system

C. Romera-Castillo [a,b,*], M. Nieto-Cid [b], C.G. Castro [b], C. Marrasé [a], J. Largier [c], E.D. Barton [b], X.A. Álvarez-Salgado [b]

[a] Institut de Ciències del Mar-CSIC, Barcelona, Spain
[b] Instituto de Investigacións Mariñas-CSIC, Vigo, Spain
[c] Bodega Marine Laboratory, University of California, Davis, CA, USA

ARTICLE INFO

Article history:
Received 15 June 2010
Received in revised form 23 December 2010
Accepted 8 February 2011
Available online 18 February 2011

Keywords:
Coloured DOM
Fluorescent DOM
Fluorescence quantum yield
Coastal upwelling

ABSTRACT

The optical properties of coloured dissolved organic matter (CDOM) – absorption coefficient, induced fluorescence, and fluorescence quantum yield – were determined in the coastal eutrophic system of the Ría de Vigo (NW Spain) under two contrasting situations: a downwelling event in September 2006 and an upwelling event in June 2007. Significantly different optical properties were recorded in the shelf surface (higher absorption coefficient and lower quantum yield) and bottom (lower absorption coefficient and higher quantum yield) waters that entered the embayment during downwelling and upwelling conditions, respectively. Continental waters presented distinctly high CDOM levels. The spatial and temporal variability of the induced fluorescence to absorption coefficient ratio during the mixing of shelf and continental waters was used to quantify the relative importance of photochemical and microbial processes under these contrasting hydrographic conditions. Photochemical processes were dominant during the downwelling episode: 86% of the variability of CDOM can be explained by photochemical degradation. On the contrary, microbial processes prevailed during the upwelling event: 77% of the total variability of CDOM was explained by microbial respiration.

1. Introduction

Coloured dissolved organic matter (CDOM) is the main UV-absorbing component in aquatic systems, contributing to prevent DNA damage in aquatic organisms, especially in a global change context of stratospheric ozone reduction (Häder and Sinha, 2005 and references therein). CDOM also absorbs radiation in the visible spectral range interfering with satellite-derived chlorophyll estimates, a fact that has stimulated the study of these materials in coastal and open ocean systems (e.g. Hoge et al., 1993; Vodacek and Blough, 1997; Siegel et al., 2002). A fraction of CDOM can emit the absorbed radiation as fluorescent light (Coble, 1996; 2007). In most estuaries and coastal areas, CDOM constitutes a dominant fraction of the DOM pool and good positive correlations are obtained between the induced fluorescence emission of CDOM, the absorption coefficient at the fluorescence excitation wavelength, and the concentration of dissolved organic carbon, DOC (e.g. Hoge et al., 1993; Vodacek et al., 1995; Vodacek and Blough, 1997; Ferrari et al., 1996; Ferrari, 2000; Del Vecchio and Blough, 2004; Del Castillo and Miller, 2008; Kowalczuk et al., 2010). In most of these cases, the more sensitive, simpler and quicker fluorescence spectroscopy measurements have been used to estimate CDOM absorption and DOC concentrations, especially for the calibration of remote sensing colour sensors. The goodness of the linear relationships between induced fluorescence and absorption coefficient, and between absorption coefficient and DOC, depends on the narrow variability of the fluorescence to absorption coefficient ratio, i.e. the fluorescence quantum yield, and the absorption coefficient to DOC ratio, i.e. the carbon specific absorption coefficient (Green and Blough, 1994; Vodacek et al., 1995). In some areas, CDOM absorption coefficient or induced fluorescence measurements can be used together with salinity to solve the mixing of three coastal water masses (e.g. Klinkhammer et al., 2000; Stedmon et al., 2010). The benefit of this approach depends on how conservative the behaviour of the optical properties of CDOM is during water mass mixing.

However, it is well known that DOC and CDOM are produced and consumed by biogeochemical processes during the mixing of water masses of contrasting origins. The most important CDOM sink is photo-degradation mediated by natural UV-light, which breaks down the coloured molecules into smaller and colourless ones (Chen and

* Corresponding author.
E-mail address: crisrc@icm.csic.es (C. Romera-Castillo).

0304-4203/$ – see front matter © 2011 Elsevier B.V. All rights reserved.
doi:10.1016/j.marchem.2011.02.001

Bada, 1992; Moran et al., 2000). On the other hand, the main source of CDOM is aerobic autotrophic and heterotrophic microbial respiration (Yentsch and Reichert, 1961; Kramer and Herndl, 2004; Nieto-Cid et al., 2006; Romera-Castillo et al., 2010) and, to a lesser extent, abiotic reactions of photo-humification (Kieber et al., 1997). DOC and CDOM absorption and fluorescence have a different response to these processes, thus altering the fluorescence quantum yield and carbon specific absorption coefficient (e.g. De Haan, 1993; Moran et al., 2000; Lønborg et al., 2010).

The in situ production of fluorescent CDOM is 5-fold the terrestrial inputs measured in the ocean interior (Yamashita and Tanoue, 2008). Although in coastal areas more affected by freshwater discharges terrestrial inputs will gain importance, net fluorescent CDOM production rates in the eutrophic embayment of the Ria de Vigo (NW Spain) still were 3-fold the continental inputs as calculated from Nieto-Cid et al. (2005). This observation, together with the dynamic nature of this coastal inlet intermittently affected by wind-driven upwelling and downwelling events (Doval et al., 1997; Álvarez-Salgado et al., 2001), makes the Ría de Vigo an excellent location to study the spatial and temporal variability of the optical properties of CDOM under contrasting hydrographic conditions and infer the relative importance of photochemical and microbial processes during the mixing of continental and oceanic waters in a coastal upwelling system.

2. Materials and methods

2.1. Survey area

The Ría de Vigo is a large (3.12 km^3) V-shaped coastal embayment in the NW Iberian Peninsula (Fig. 1). The River Oitaben–Verdugo is the main freshwater source, with an average annual flow of 15 $m^3\ s^{-1}$ (Gago et al., 2005). It drains into San Simon Bay, a sedimentary basin in the innermost part of the embayment. The mouth of the ría, where it opens to the Atlantic Ocean, is divided by the Cíes Islands into northern (2.5 km wide, 25 m deep) and southern (5 km wide, 60 m deep) entrances. The hydrography of the Ría de Vigo is dictated by coastal wind stress, which is upwelling-favourable from April–May to September–October and downwelling-favourable the rest of the year (Wooster et al., 1976; Torres et al., 2003). The upwelling-favourable season appears as a succession of wind stress/relaxation cycles of period 10–20 days (Álvarez-Salgado et al., 1993), when the cold nutrient-rich and DOC-poor Eastern North Atlantic Central Water (ENACW) enters the ría (Doval et al., 1997; Álvarez-Salgado et al., 2001; Nieto-Cid et al., 2005). The transition from the upwelling- to the downwelling-favourable seasons occurs from mid September to mid October and it is characterised by the entry of warm, nutrient-poor and DOC-rich shelf surface waters into the ría (Doval et al., 1997; Álvarez-Salgado et al., 2001; Nieto-Cid et al., 2005). Whereas during the upwelling-favourable season the microplankton community (>20 μm) is dominated by diatoms and the net community metabolism is autotrophic, in the transition from the upwelling- to the downwelling-favourable season dinoflagellates prevail and the metabolism is balanced or net heterotrophic (Figueiras and Ríos, 1993; Cermeño et al., 2006; Piedracoba et al., 2008).

2.2. Sampling programme

Water samples were collected aboard R/V Mytilus during two contrasting periods: from 26 to 30 September 2006, during the transition from the upwelling- to the downwelling-favourable season, and from 25 to 28 June 2007, during the upwelling season. On 26 and 30 September 2006 and 25 and 28 June 2007, the twelve stations indicated in Fig. 1 were visited. On 28 September 2006 and 27 June 2007 the sampling concentrated on the middle sector (stns A3, B3 and C3), on 27 September 2006 in the outer sector (stns A5, B5 and C5), and on 29 September 2006 on the inner sector (stns A2, B2 and C2) of the Ría de Vigo. Surface samples were taken from the continuous non-toxic underwater supply at 2 m depth. At stations B0, B1, B2, B3, B4 and B5 full-depth continuous conductivity–temperature–depth (CTD) profiles were recorded with a SBE 9/11 CTD probe incorporated into a rosette sampler equipped with twelve 12-L Niskin bottles. Conductivity measurements were converted into practical salinity scale values with the equation of UNESCO (1985). Water samples from 3 to 5 depths were collected depending on the bathymetry of the stations.

Aliquots for the analysis of dissolved oxygen (O_2), nutrient salts (NH_4^+, NO_2^-, NO_3^-, HPO_4^{2-} and H_4SiO_4), dissolved organic carbon (DOC), absorbance and fluorescence of coloured dissolved organic matter (CDOM) were collected from both the non-toxic underwater pipe and the Niskin bottles.

Coastal wind data over the study periods (Fig. 1) were obtained from a mooring located about 60 km offshore of Cabo Silleiro ran by

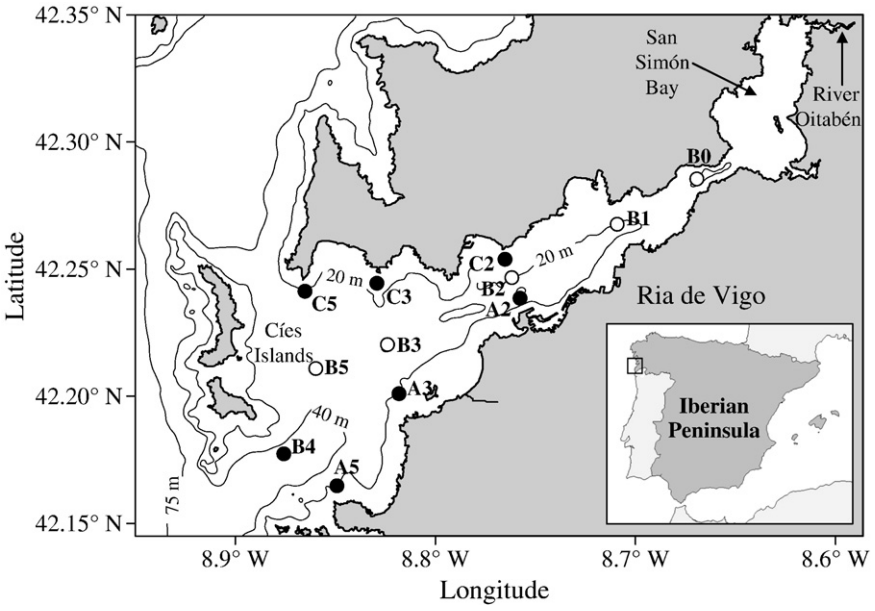

Fig. 1. Map showing the bathymetry and location of sampling stations in the Ría de Vigo (NW Spain).

Spanish Port Authority (Puertos del Estado, http://www.puertos.es). Hourly data were checked for outliers, and any gaps of less than 6 h were filled by interpolation with a cubic spline before the series was low pass filtered to remove periods less than 40 h and then sub-sampled to produce 6 hourly series.

Temperature observations were available from TidBit thermistor loggers and SeaBird MicroCat SBE37 recorders moored at 42° 12.4′N, 8° 48.6′W in 21 m depth, close to stn A3 on the southern side of the central ría (Fig. 1). The data were compared with CTD profiles made at the site to check that accuracy lay within the quoted manufacturers' specifications. The TidBits have a nominal accuracy of ±0.2 °C and precision of ±0.02 °C, while the MicroCats have quoted values of ± 0.002 °C precision and ±0.0001 °C resolution. The temperature series, recorded at 2 min intervals, were edited for outliers before averaging to 1 h intervals.

2.3. Chemical analysis

Dissolved oxygen was determined by the Winkler method with potentiometric endpoint detection using a Titrino 72′ analyser (Metrohm) with an analytical precision of ±0.5 μmol kg^{-1}. Oxygen concentrations were referred to the oxidation state of nitrate (O_2cor) by considering that the ammonium and nitrite of the samples were oxidised to nitrate. Since 0.5 mol of oxygen is necessary to oxidise 1 mol of nitrite to nitrate and 2 mol of oxygen is required to oxidise 1 mol of ammonium to nitrate.

$$O_2\mathrm{cor} = O_2 - \frac{1}{2}\cdot NO_2^- - 2\cdot NH_4^+ \quad (1)$$

This correction allows comparison of dissolved oxygen consumption versus nutrient salts and CDOM production independently of the oxidation state of the inorganic nitrogen form involved in the organic matter mineralisation process. The corrected Apparent Oxygen Utilisation (AOU), i.e. the difference between the dissolved oxygen concentration at saturation and the actual corrected oxygen concentration of the sample, was calculated following UNESCO (1986).

Samples for nutrient salts analysis were collected in 50 mL polyethylene bottles and preserved at 4 °C until determination in the base laboratory within 4 h of collection using standard segmented flow analysis (SFA) procedures. The precisions of the methods are ±0.02 μmol kg^{-1} for nitrite, ±0.1 μmol kg^{-1} for nitrate, ±0.05 μmol kg^{-1} for ammonium, ±0.02 μmol kg^{-1} for phosphate and ±0.05 μmol kg^{-1} for silicate.

Samples for DOM analyses were taken in 500 mL acid-washed glass flasks and transported into the base laboratory within 4 h of collection. Once in the laboratory, aliquots for DOC, and absorbance and fluorescence of CDOM were immediately filtered through precombusted (450 °C, 4 h) Whatman GF/F filters in an acid-cleaned all-glass filtration system, under positive pressure with low N_2 flow.

Approximately 10 mL of the filtrate were collected for DOC determination in precombusted (450 °C, 12 h) glass ampoules. These samples were acidified with H_3PO_4 to pH<2 and the ampoules were heat-sealed and stored in the dark at 4 °C until analysis. DOC was measured with a Shimadzu TOC-CVS organic carbon analyser. The system was standardised daily with potassium hydrogen phthalate. The concentration of DOC was determined by subtracting the instrument blank area from the average peak area and dividing by the slope of the standard curve. The precision of the equipment was ±0.7 μmol L^{-1}. The accuracy was tested daily with the DOC reference materials provided by Prof. D.A. Hansell (Miami University). We obtained average concentrations of 45.7 ± 1.6 μmol L^{-1} for the deep ocean reference (Sargasso Sea deep water, 2600 m) minus blank reference materials. The nominal DOC value provided by the reference laboratory is 44.0 ± 1.5 μmol L^{-1}.

2.4. Optical measurements

Absorbance of CDOM was measured within 4 h of collection using a Beckman Counter DU 800 spectrophotometer equipped with a 10 cm quartz round cell. Spectral scans were collected in a wavelength range of 250–700 nm at a constant room temperature of 25 °C. Pre-filtered (0.2 μm) Milli-Q water was used as the reference for all samples. Absorption coefficients were calculated using the equation:

$$a_{\mathrm{CDOM}}(\lambda) = \frac{2.303}{l}\cdot \mathrm{ABS}(\lambda) \quad (2)$$

where ABS(λ) is the absorbance at wavelength λ, and l is the cell length in metres.

Using the Levenberg–Marquardt algorithms implemented in the Stat Soft Inc. STATISTICA software we obtained the coefficients a_{CDOM}(340), S and K that best fit the equation:

$$a_{\mathrm{CDOM}}(\lambda) = a_{\mathrm{CDOM}}(340)\cdot\exp(-S\cdot(\lambda-340)) + K \quad (3)$$

where $a_{\mathrm{CDOM}}(340)$ is the absorption coefficient at wavelength 340 nm (in m^{-1}), S is the spectral slope (in nm^{-1}) and K is a background constant caused by residual scattering by fine size particle fractions, micro-air bubbles or colloidal material present in the sample, refractive index differences between sample and the reference, or attenuation not due to organic matter (in m^{-1}). The estimated detection limit of this spectrophotometer is 0.001 absorbance units or 0.02 m^{-1}. The carbon specific CDOM absorption coefficient at 340 nm, $a^*_{\mathrm{CDOM}}(340)$, was calculated dividing $a_{\mathrm{CDOM}}(340)$ by the DOC concentration.

Induced fluorescence of CDOM (FDOM) was measured after 4 h of collection with a Perkin Elmer LS 55 luminescence spectrometer, equipped with a xenon discharge lamp, equivalent to 20 kW for 8 μs duration. The detector was a red-sensitive R928 photomultiplier and a photodiode worked as reference detector. Slit widths were 10.0 nm for the excitation and emission wavelengths. Measurements were performed at a constant room temperature of 25 °C in a 1 cm quartz fluorescence cell. MQ water was used as a reference blank for fluorescence analysis. Fluorescence intensity was measured at a fixed excitation/emission wavelength of 340 nm/440 nm, F(340/440), which is characteristic of humic-like substances (Coble, 1996). The spectrofluorometer was calibrated daily with quinine sulphate in 0.1 N sulphuric acid. F(340/440) was expressed in μg L^{-1} of quinine sulphate, hereafter quinine sulphate units (QSU). The equivalent concentration of each peak was determined by subtracting the MQ blank peak height from the sample average peak height, and dividing by the slope of the standard curve. The precision was ±0.1 QSU.

The quantum yield of fluorescence at 340 nm, $\Phi(340)$, is the portion of the light absorbed at 340 nm, $a_{\mathrm{CDOM}}(340)$, that is re-emitted as fluorescent light. $\Phi(340)$, for the samples was determined using the ratio of the absorption coefficient at 340 nm and the corresponding fluorescence emission between 400 and 600 nm from the quinine sulphate standard in 0.1 N H_2SO_4 using the equation (Green and Blough, 1994):

$$\Phi(340) = \frac{F(400-600)}{a_{\mathrm{CDOM}}(340)}\cdot\frac{a_{\mathrm{CDOM}}(340)_{\mathrm{QS}}}{F(400-600)_{\mathrm{QS}}}\cdot\Phi(340)_{QS} \quad (4)$$

where $a_{\mathrm{CDOM}}(340)$ and $a_{\mathrm{CDOM}}(340)_{\mathrm{QS}}$ are the absorption coefficients of the sample and the QS standard (in m^{-1}), respectively; F(400–600) and $F(400–600)_{\mathrm{QS}}$ are the average integrated fluorescence spectra between 400 and 600 nm at a fixed excitation wavelength of 340 nm (in μg QS L^{-1}) of the sample and the QS standard, respectively; and $\Phi(340)_{QS}$ is the dimensionless fluorescence quantum yield of the QS standard, equal to 0.54 according to Melhuish (1961).

Although fluorescence spectra between 400 and 600 nm, F(400–600), were recorded in 34 out of the 197 samples collected in the Ría

de Vigo, the very good linear correlation between $F(340/440)$ and $F(400–600)$ ($R^2 = 0.87$, $n = 34$, $p<0.001$) reveals that $F(400–600)$ can be estimated from $F(340/440)$ using the dimensionless conversion factor of 0.62 ± 0.05. Therefore, the ratio $F(400–600)/a_{CDOM}(340)$ can be obtained from the ratio $F(340/440)/a_{CDOM}(340)$ for all the samples collected in this study, in such a way that Eq. (4) can be rewritten as:

$$\Phi(340) = \beta \cdot \Phi(340)_{QS} \cdot \frac{F(340/440)}{a_{CDOM}(340)} = 2.2(\pm 0.2) \cdot 10^{-3} \cdot \frac{F(340/440)}{a_{CDOM}(340)} \quad (5)$$

where $\beta = 4.2(\pm 0.3)\ 10^{-3}\ m^{-1}\ QSU^{-1}$ is a constant that accounts for the conversion factor $F(400–600)/F(340/440)$ and for the $F(400–600)_{QS}/a_{CDOM}(340)_{QS}$ ratio.

3. Results

3.1. Hydrography and dynamics of the Ría de Vigo in September 06 and July 07

From 25 to 30 September 2006 coastal winds evolved from northerly to southerly, i.e. from upwelling- to downwelling-favourable (Fig. 2a). Concomitantly, water temperature at stn A3 (Fig. 2b) traced the replacement of water colder than 16.8 °C (top 25 m) on 25 September by warmer shelf surface water >18 °C (top 25 m) on 30 September. The evolution of surface temperature from 25 September (Fig. 3a) to 30 September (Fig. 3b), indicates that the transition from upwelling- to downwelling favourable winds was not a local phenomenon observed only at stn A3. It affected the entire ría from surface to bottom, and from the outer to the inner segment of the embayment. Salinity varied in a very narrow range, from 35.1 in the surface inner ría (Fig. 3c and d) to 35.7 in the bottom outer ría (not shown).

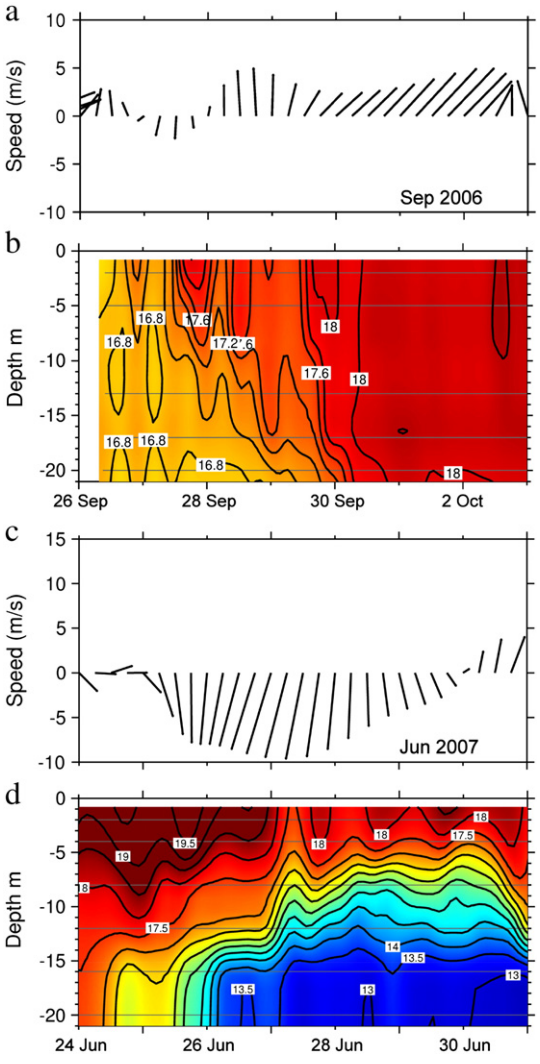

Fig. 2. Coastal winds (a and c) and thermistor records (b and d) at stn A3 during the September 06 and June 07 sampling periods.

From 25 to 28 June 2007, as a response to the strong northerly winds that were blowing on the shelf (Fig. 2c), the cold (<13 °C) and salty (>35.7) Eastern North Atlantic Central Water (ENACW) entered the ría through the bottom of the southern mouth. Cooling due to upwelling was perceptible when comparing the sea surface temperature distributions of 25 June (Fig. 3e) and 28 June (Fig. 3f). The 14 °C isotherm was at >30 m depth on 25 June, and reached 15 m depth three days later (Fig. 4a and b). Salinity exhibited in this case a wider range of variability, from 31.1 in the surface inner ría (Fig. 3g and h) to 35.9 in the bottom outer ría (not shown). The warmer and fresher waters observed in the inner ría are the result of the mixing of the oceanic ENACW with the continental waters carried by the River Oitaben–Verdugo, which represent >5% in samples of salinity <34.

3.2. Nutrient status under contrasting hydrographic conditions

Shelf surface waters that entered the ría during the downwelling event sampled in September 06 were nutrient-poorer than the waters inside the ría (Fig. 5a and b). Phosphate and silicate distributions (not shown) followed a parallel pattern to the total inorganic nitrogen (TIN) distribution, presenting significant linear correlations ($r^2 = 0.74$, $n = 112$, $p<0.001$ and $r^2 = 0.69$, $n = 112$, $p<0.001$) for phosphate and silicate, respectively. The predominant form of inorganic nitrogen was ammonium, which represented $81 \pm 2\%$ of TIN (Eq. 1 in Table 1), i.e. pointing to a system dominated by recycled production (Eppley and Peterson, 1979). This contrasts with the negative values of AOU in the nutrient-poor shelf surface waters that entered the ría, lower than those of the water in the inner part of the ría, where positive values of AOU were recorded (Fig. 5c and d). The distribution of DOC (Fig. 5e and f) was more complex: on 25 September, a strong gradient was observed between the DOC-rich (>100 μmol L^{-1}) surface waters coming from the sedimentary basin of San Simon Bay and the DOC-poor (<65 μmol L^{-1}) waters of the bottom outer ría. On 30 September, shelf surface waters, which have an intermediate DOC concentration (about 80 μmol L^{-1}), modified the DOC distribution of the ría.

During the event sampled on June 07, the upwelling of nutrient-rich and dissolved oxygen-poor oceanic ENACW produced a clear impact on the distributions of total inorganic nitrogen (Figs. 4c and d and 6a and b) and AOU (Figs. 4e and f and 6c and d). Nitrate was the predominant inorganic nitrogen form in this case, representing $82 \pm 3\%$ of TIN (Eq. 2 in Table 1), which is characteristic of a system dominated by new production (Eppley and Peterson, 1979). The DOC distributions of June 07 (Figs. 4g and h and 6e and f) traced the entry of the DOC-poor (<68 μmol L^{-1}) oceanic ENACW. The signal of the River Oitaben–Verdugo after crossing San Simón bay is also visible in the surface innermost stations, where a DOC value of 112 μmol L^{-1} was recorded.

3.3. Optical properties of CDOM under contrasting hydrographic conditions

During the downwelling event sampled in September 06, the DOC-rich waters coming from the sedimentary basin of San Simón bay presented the highest values of $a_{CDOM}(340)$, >0.77 m^{-1} (Fig. 7a and b). Shelf surface waters were characterised by much lower values of $a_{CDOM}(340)$, 0.34 ± 0.02 m^{-1} (average ± SD of the surface sample at stn B5).

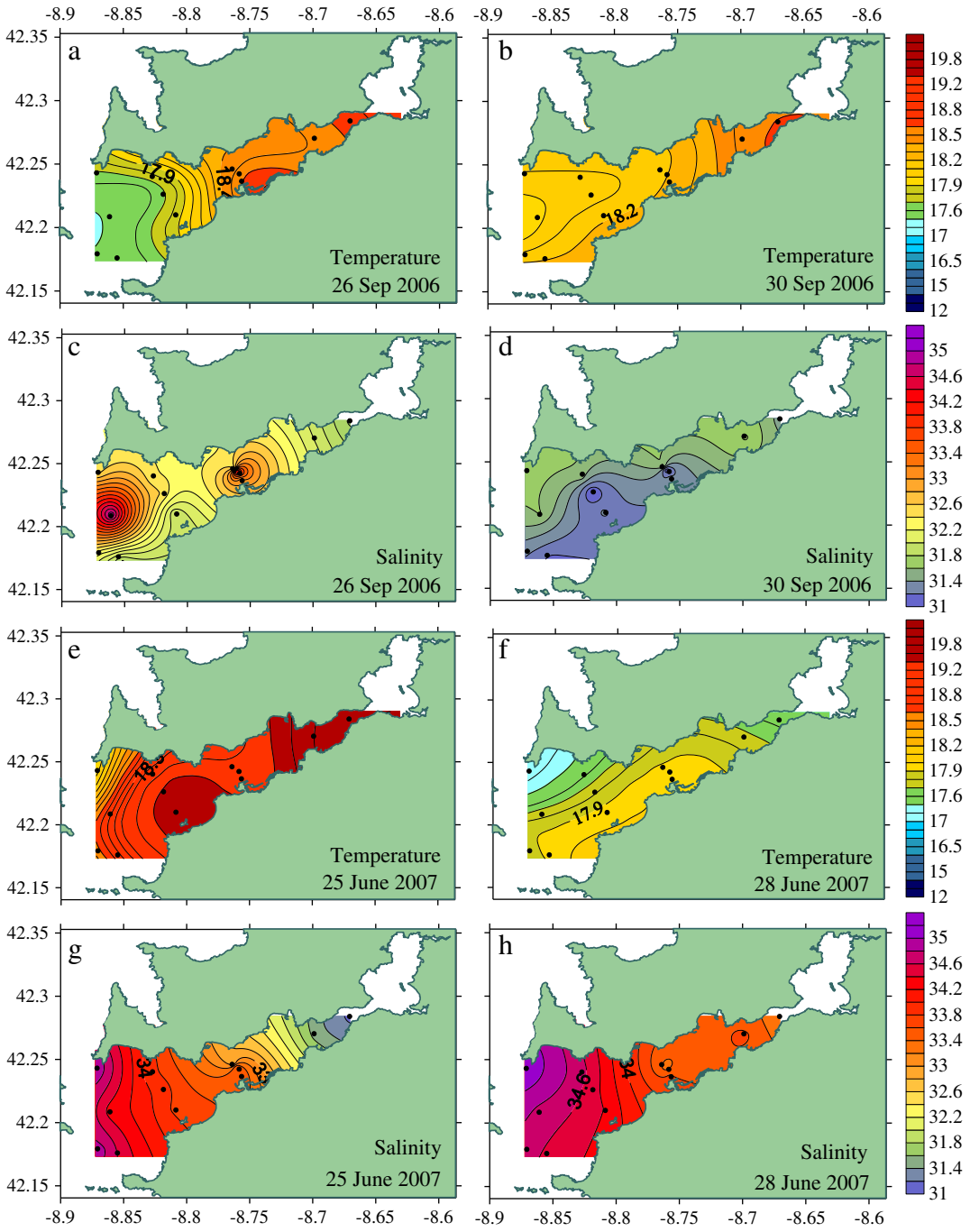

Fig. 3. Sea surface distribution for September 26 and 30 (2006) of temperature (a and b) and salinity (c and d) and sea surface distribution for June 25 and 28 (2007) of temperature (e and f) and salinity (g and h). Temperature in °C.

On the contrary, $\Phi(340)$ were not that different: $0.82 \pm 0.03\%$ for the surface sample of stn B0 and $0.76 \pm 0.02\%$ for the surface sample of stn B5 (Fig. 7c and d). The distribution of $F(340/440)$ (data not shown) was parallel to $a_{CDOM}(340)$: $r^2 = 0.79$, $n = 112$, $p < 0.001$. The surface distribution of $a_{CDOM}(340)$ on 25 September shows the mixing of the coloured waters from the inner ría with the bleached waters from the adjacent shelf (Figs. 4i and 8a). Five days later, the surface layer of the ría reflected the intrusion of CDOM-poor shelf surface waters into the inner ría (Figs. 4j and 8b). Similar patterns are observed in the distributions of $\Phi(340)$ (Figs. 4k and l and 8c and d).

During the upwelling event sampled on June 07, the oceanic ENACW cooler than 14 °C that occupied the bottom of the ría presented relatively low $a_{CDOM}(340)$ but high $\Phi(340)$ values, 0.23 ± 0.04 m^{-1} and $1.2 \pm 0.3\%$ respectively (Fig. 4i–l), compared with the warmer waters in the ría before the upwelling episode. The influence of the CDOM transported by the River Oitaben–Verdugo through San Simon Bay can also be traced in the low salinity water of the innermost part of the ría, where an $a_{CDOM}(340)$ value of 1.82 m^{-1} was recorded. The highest values of $\Phi(340)$, $1.6 \pm 0.1\%$, were observed in the inner ría, below 10 m on 28 June. This maximum is coincident with the maxima observed in TIN (Fig. 4d) and AOU (Fig. 4f). In this case, the linear correlation of $F(340/440)$ with $a_{CDOM}(340)$ was lower than in September 06 ($r^2 = 0.60$, $n = 80$, $p < 0.001$) when the outlying samples B0 (2 m) on 25 June and B3 (20 m) on 27 June are excluded from the analysis.

Absorption spectral slopes, S (not shown), were not significantly different during the upwelling and downwelling periods: they ranged

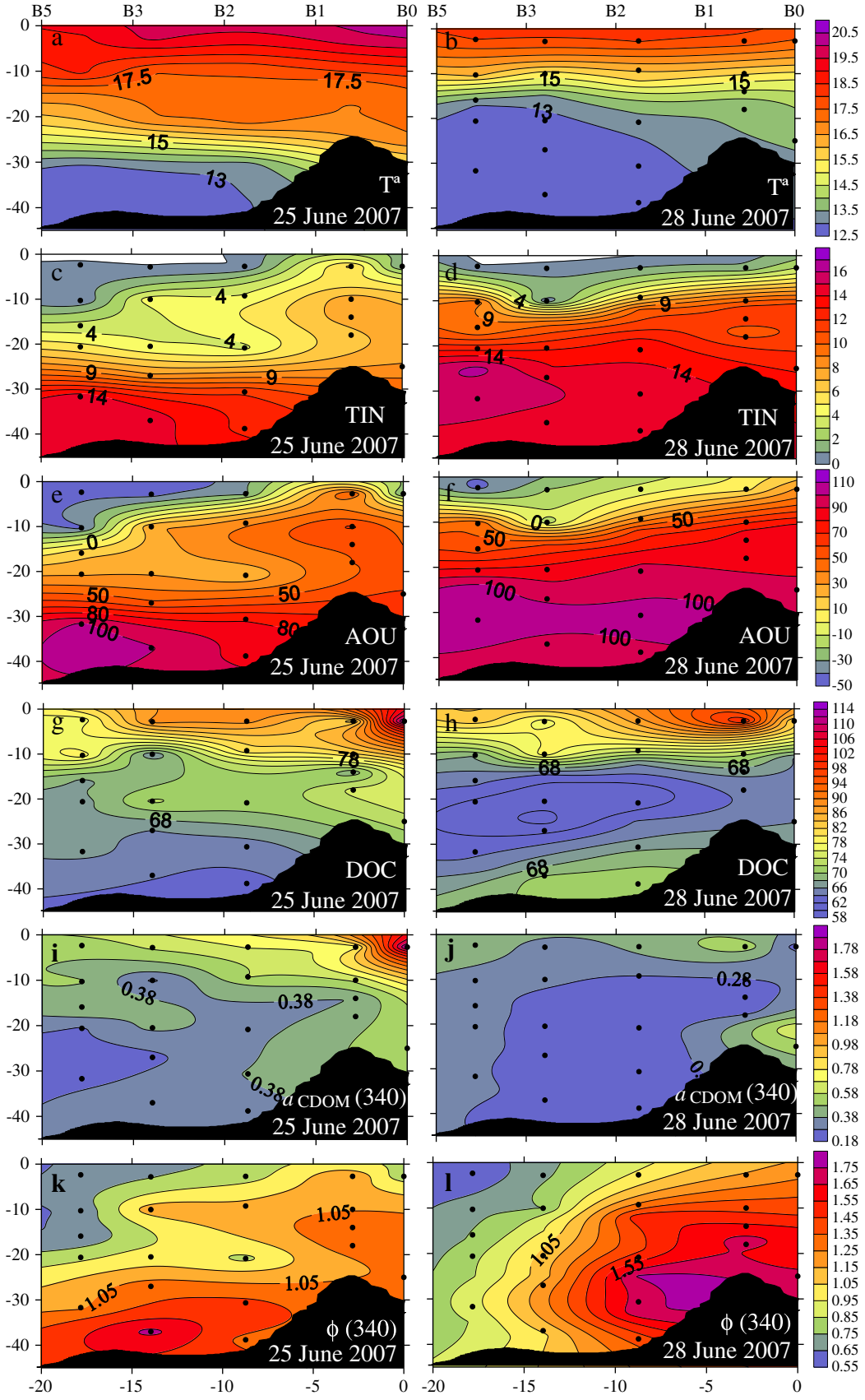

Fig. 4. Vertical distributions for June 25 and 28 (2007) of temperature (a, b) in °C; total inorganic nitrogen (TIN) (c and d) in μmol L^{-1}; apparent oxygen utilization (AOU) (e and f) in μmol kg^{-1}; dissolved organic carbon (DOC) (g and h) in μmol L^{-1}; CDOM absorption coefficient at 340 nm, $a_{CDOM}(340)$ (i and j), in m^{-1} and CDOM fluorescence quantum yield at 340 nm, $\Phi(340)$ (k and l). X-axis is distance from station B0.

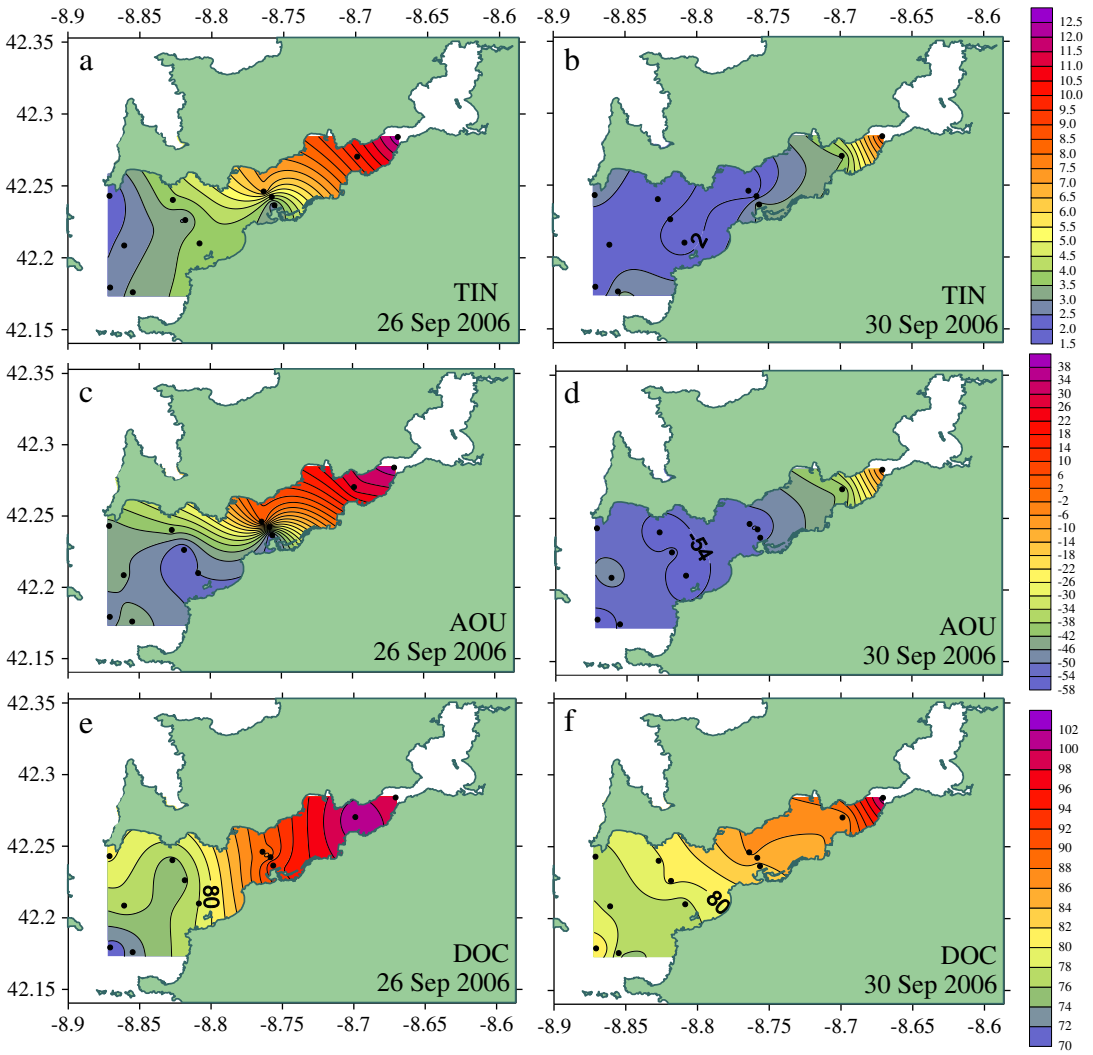

Fig. 5. Sea surface distributions for September 26 and 30 (2006) of total inorganic nitrogen (TIN) (a and b) in μmol L^{-1}; apparent oxygen utilization (AOU) (c and d) in μmol kg^{-1} and dissolved organic carbon (DOC) (e and f) in μmol L^{-1}.

between 0.018 nm^{-1} and 0.023 nm^{-1} during the former and between 0.018 nm^{-1} and 0.024 nm^{-1} during the latter period. S varied inversely to $a_{CDOM}(340)$ but the log transformed plot of the two variables (Fig. 9) shows that the slope of the relationship between *S* and $a_{CDOM}(340)$ (regression model II; Sokal and Rohlf, 1995) was significantly higher for the downwelling (-0.26 ± 0.01) than for the upwelling period (-0.16 ± 0.01). For the case of the upwelling period, the two outlying samples (grey dots) were not considered. If they are included in the analysis the determination coefficient of the relationship increases ($r^2 = 0.76$) but the origin intercept and slope of the regression does not change significantly.

4. Discussion

4.1. Optical properties of CDOM in the Ría de Vigo: comparison with other marine systems

The average ± SD values of the absorption coefficient, $a_{CDOM}(340)$, and carbon-specific CDOM absorption coefficient, $a^*_{CDOM}(340)$, at 340 nm in the Ría de Vigo were significantly higher ($p<0.001$) during the downwelling (0.43 ± 0.11 m^{-1} and 5.4 ± 1.1 m^2 mol C^{-1}) than during the upwelling event (0.35 ± 0.14 m^{-1} and 4.5 ± 1.3 m^2 mol C^{-1}). On the contrary, $\Phi(340)$ was significantly lower ($p<0.001$) during the downwelling ($0.81 \pm 0.11\%$) than during the upwelling episode ($1.03 \pm 0.30\%$, Table 2). Day and Faloona (2009) also found less coloured surface waters in association with intense upwelling episodes in the Northern California coast. The distributions of $a_{CDOM}(\lambda)$ and $a^*_{CDOM}(\lambda)$ in the Ría de Vigo, resulting from the mixing of DOC and CDOM-rich continental waters with DOC and CDOM-poor ocean waters, are characteristic of most coastal systems (e.g. Vodacek and Blough, 1997; Chen et al., 2002; Del Vecchio and Blough, 2004). This mixing pattern results in a decrease of $a_{CDOM}(\lambda)$ with depth. However, in other coastal upwelling regions drier and more irradiated than the NW Iberian Peninsula, $a_{CDOM}(\lambda)$ tends to increase with depth (Coble et al., 1998; Kudela et al., 2006).

The variety of wavelengths used in the literature to determine $a_{CDOM}(\lambda)$ – 325, 355, 375 and 443 nm being the most common – makes difficult the direct comparison of this parameter obtained in the Ría de Vigo with other marine systems. In this work, we have used $a_{CDOM}(340)$ to allow the quantitative estimation of $\Phi(340)$ referred to a quinine sulphate standard of known fluorescence quantum yield. In any case, average ± SD values for the referred wavelengths are reported in Table 2. The significant difference observed in $a_{CDOM}(340)$ between the upwelling and the downwelling episodes sampled in this study (see above) is also observed for the other wavelengths. The average ± SD values of $a_{CDOM}(325)$, $a_{CDOM}(355)$, $a_{CDOM}(375)$ and

Table 1
Coefficients of selected linear regression equations for the two periods studied in the Ría de Vigo.

N°	Period	Equation	R^2	p	n
1	Downwelling	$NH_4^+ = -1.2(\pm0.1) + 0.81(\pm0.02) \cdot TIN$	0.92	<0.001	109
2	Upwelling	$NO_3^- = -0.8(\pm0.2) + 0.82(\pm0.03) \cdot TIN$	0.94	<0.001	80
3	Downwelling	$DOC = 50(\pm2) + 65(\pm7) \cdot a_{CDOM}(340)$	0.46	<0.001	106
4	Upwelling	$DOC = 48(\pm2) + 76(\pm5) \cdot a_{CDOM}(340)$	0.75	<0.001	77
5	Downwell + Upwell	$DOC = 49(\pm1) + 69(\pm4) \cdot a_{CDOM}(340)$	0.63	<0.001	183
6	Downwelling	$F^*(340/440) = -10(\pm7) + 0.32(\pm0.20) \cdot salinity$	0.024	n.s.	109
7	Downwelling	$a^*_{CDOM}(340) = 1.7(\pm1.6) - 0.04(\pm0.05) \cdot salinity$	0.006	n.s.	109
8	Downwelling	$AOU = -2865(\pm342) + 80\ (\pm10) \cdot salinity$	0.39	<0.001	109
9	Upwelling	$F^*(340/440) = 15\ (\pm2) - 0.39(\pm0.05) \cdot salinity$	0.43	<0.001	80
10	Upwelling	$a^*_{CDOM}(340) = 5.0\ (\pm0.3) - 0.13(\pm0.01) \cdot salinity$	0.74	<0.001	80
11	Upwelling	$AOU = -1227\ (\pm153) + 36\ (\pm4) \cdot salinity$	0.46	<0.001	80
12	Downwell + Upwell	$\Delta F^*(340/440) = 4.8(\pm0.4) \cdot \Delta a^*_{CDOM}(340)$	0.46	<0.001	189
13	Downwelling	$\Delta F^*(340/440) = 0.005(\pm0.001) \cdot \Delta AOU + 2.8(\pm0.3) \cdot \Delta a^*_{CDOM}(340)$ $\beta_1 = 0.27 \pm 0.07 \cdot \beta_2 = 0.66 \pm 0.07$	0.77	<0.001	109
14	Upwelling	$\Delta F^*(340/440) = 0.008(\pm0.001) \cdot \Delta AOU + 2.1(\pm0.4) \cdot \Delta a^*_{CDOM}(340)$ $\beta1 = 0.66 \pm 0.07 \cdot \beta2 = 0.36 \pm 0.07$	0.63	<0.001	80

(n.s.) not significant.

$a_{CDOM}(443)$ recorded in the Ría de Vigo for both periods – $0.54 \pm 0.17\ m^{-1}$, $0.29 \pm 0.10\ m^{-1}$, $0.20 \pm 0.07\ m^{-1}$ and $0.051 \pm 0.023\ m^{-1}$ (Table 2), respectively – are higher than in continental shelf surface waters but lower than in estuaries and coastal inlets affected by important freshwater inputs (e.g. Vodacek and Blough, 1997; Ferrari, 2000; Babin et al., 2003; Del Vecchio and Blough, 2004; Nelson et al., 2010; Kowalczuk et al., 2010). Our surface values of $a_{CDOM}(\lambda)$ are in the upper end of those reported in other coastal upwelling regions such as Northern California (Day and Faloona, 2009), Mauritania (Bricaud et al., 1981) or Arabia (Coble et al., 1998). They are also significantly higher than in coastal oligothrophic sites such as the Blanes Bay Observatory in the NW Mediterranean, where $a_{CDOM}(325)$ was $0.28 \pm 0.09\ m^{-1}$ and $a_{CDOM}(443)$ was $0.016 \pm 0.015\ m^{-1}$ (average ± SD) over an annual cycle (Romera-Castillo et al., unpub. data) and in oligotrophic open ocean waters (Nelson et al., 2004, 2007, 2010; Swan et al., 2009).

As for the case of $a_{CDOM}(\lambda)$, direct comparison of absolute values of S obtained by different authors is difficult because they have used different fitting procedures across different wavelength ranges and S slightly differs depending on those choices (Ferrari, 2000; Stedmon et al., 2000; Blough and Del Vecchio, 2002). In our case, spectral slopes were determined over the range 250–500 nm, and the observed values, $0.0205 \pm 0.0013\ nm^{-1}$ (average ± SD), are close to those reported by Babin et al. (2003), $0.0176 \pm 0.0020\ nm^{-1}$ (average ± SD; wavelength range 350–750 nm),who considered a wide variety of coastal and open ocean systems. Our values are also between those reported by Ferrari (2000) for surface open ocean ($0.025\ nm^{-1}$ and more) and coastal waters ($0.013–0.018\ nm^{-1}$) calculated over a wavelength range of 350–480 nm. Bricaud et al. (1981) obtained lower S mean values, $0.0150 \pm 0.0023\ nm^{-1}$, in the Mauritanian upwelling region for a wavelength range of 375–500 nm.

Although absolute values of S are not directly comparable, some common trends can be defined. This is the case of the inverse relationship between S and $a_{CDOM}(\lambda)$ reported in our Fig. 9, which is observed in most coastal and open ocean waters (e.g. Del Castillo and Coble, 2000; Stedmon et al., 2000; Stedmon and Markager, 2001; Nelson et al., 2010). In general, i) CDOM of terrestrial origin is characterised by lower spectral slopes than CDOM of marine origin; ii) microbial degradation processes lowers; and iii) photodegradation rises the spectral slopes (Del Vecchio and Blough, 2004; Nelson et al., 2007, 2010). With these considerations in mind, the remarkably higher slope of the relationship between $a_{CDOM}(340)$ and S for September 06 compared with June 07 suggests a dominance of photodegradation over microbial processes during the downwelling period and the contrary during the upwelling period, especially considering that the effect of continental waters (that would tend to lower the slopes) is larger during the upwelling period.

The concentration of DOC correlated with $a_{CDOM}(340)$ for both periods (Eqs. 3 and 4, Table 1). Eqs. (3) and (4) are not significantly different, neither in the y-intercept nor in the slope. Therefore, the relationship between DOC and $a_{CDOM}(340)$ can be presented under an unique regression equation (Eq. 5, Table 1). The y-intercept, $49 \pm 1\ \mu mol\ L^{-1}$, represents the colourless DOC. Since the average ± SD concentration of DOC for all the samples taken in the Ría de Vigo in September 2006 and June 2007 is $77 \pm 13\ \mu mol\ L^{-1}$, the coloured DOC would represent 36 ± 20% of the bulk DOC. This value is within the range of the characteristic values for open ocean, approx. 20%, and coastal areas, up to 70% (e.g. Ferrari et al., 1996; Del Vecchio and Blough, 2004; Coble, 2007; Kowalczuk et al., 2010). That appears reasonable because wind-driven upwelling/downwelling systems are coastal areas with enhanced oceanic influence. The inverse of the slope of Eq. 5 (Table 1), 14.5 (±0.8) $m^2\ mol\ C^{-1}$, represents the mean value of the DOC specific absorption coefficient, $a^*_{CDOM}(340)$, for the coloured DOC fraction. Using the factor 0.74 ± 0.02 (to convert $a_{CDOM}(340)$ into $a_{CDOM}(355)$), the mean specific CDOM absorption coefficient of the coloured DOC of Ría de Vigo at 355 nm, $a^*_{CDOM}(355)$, results $20 \pm 1\ m^2\ mol\ C^{-1}$, a relatively high value compared with other coastal areas. $a^*_{CDOM}(355)$ for the coloured DOC in Middle Atlantic Bight samples with $a_{CDOM}(355) < 1\ m^{-1}$ (reduced river plume influence) ranged from 8 to 18 $m^2\ mol\ C^{-1}$ (Del Vecchio and Blough, 2004). Regression slopes larger than 20 $m^2\ mol\ C^{-1}$ are obtained only for samples with $a_{CDOM}(355) > 1\ m^{-1}$ (strong river plume influence). Ferrari et al. (1996) also reported relatively low values of $a^*_{CDOM}(355)$, around 14–15 $m^2\ mol\ C^{-1}$, in the Southern Baltic Sea, where $a_{CDOM}(355)$ was always above $1\ m^{-1}$. Lower specific absorption coefficient, 16 $m^2\ mol\ C^{-1}$, were also obtained by Vodacek and Blough (1997) in Delaware Bay. In the Gulf of Lions (NW Mediterranean), $a^*_{CDOM}(355)$ ranged from $4 \pm 2\ m^2\ mol\ C^{-1}$ in surface marine waters to $23 \pm 7\ m^2\ mol\ C^{-1}$ in the river Rhone plume (Ferrari, 2000). On the contrary, a much higher value of $a^*_{CDOM}(355)$, $32 \pm 1\ m^2\ mol\ C^{-1}$, was obtained by Kowalczuk et al. (2010) in the South Atlantic Bight, where $a_{CDOM}(355)$ up to $20\ m^{-1}$ were recorded.

It has been shown in the results section that $F(340/440)$ correlated significantly with $a_{CDOM}(340)$ in the Ría de Vigo during the two study periods. A good linear correlation between the fluorescence emission of CDOM and the absorption coefficient at the fluorescence excitation wavelength has been found in most coastal areas, allowing the estimation of absorption coefficients from fluorescence measurements (e.g. Hoge et al., 1993; Vodacek et al., 1995; Vodacek and Blough, 1997; Ferrari et al., 1996; Ferrari, 2000; Del Vecchio and Blough, 2004; Kowalczuk et al., 2010). This is because the variability of $\Phi(\lambda)$ is usually at least one order of magnitude lower than the variability of $a(\lambda)$ (Green and Blough, 1994). Our values of $\Phi(340)$, which range from 0.56% to 1.76%, were close to the 1% reported by

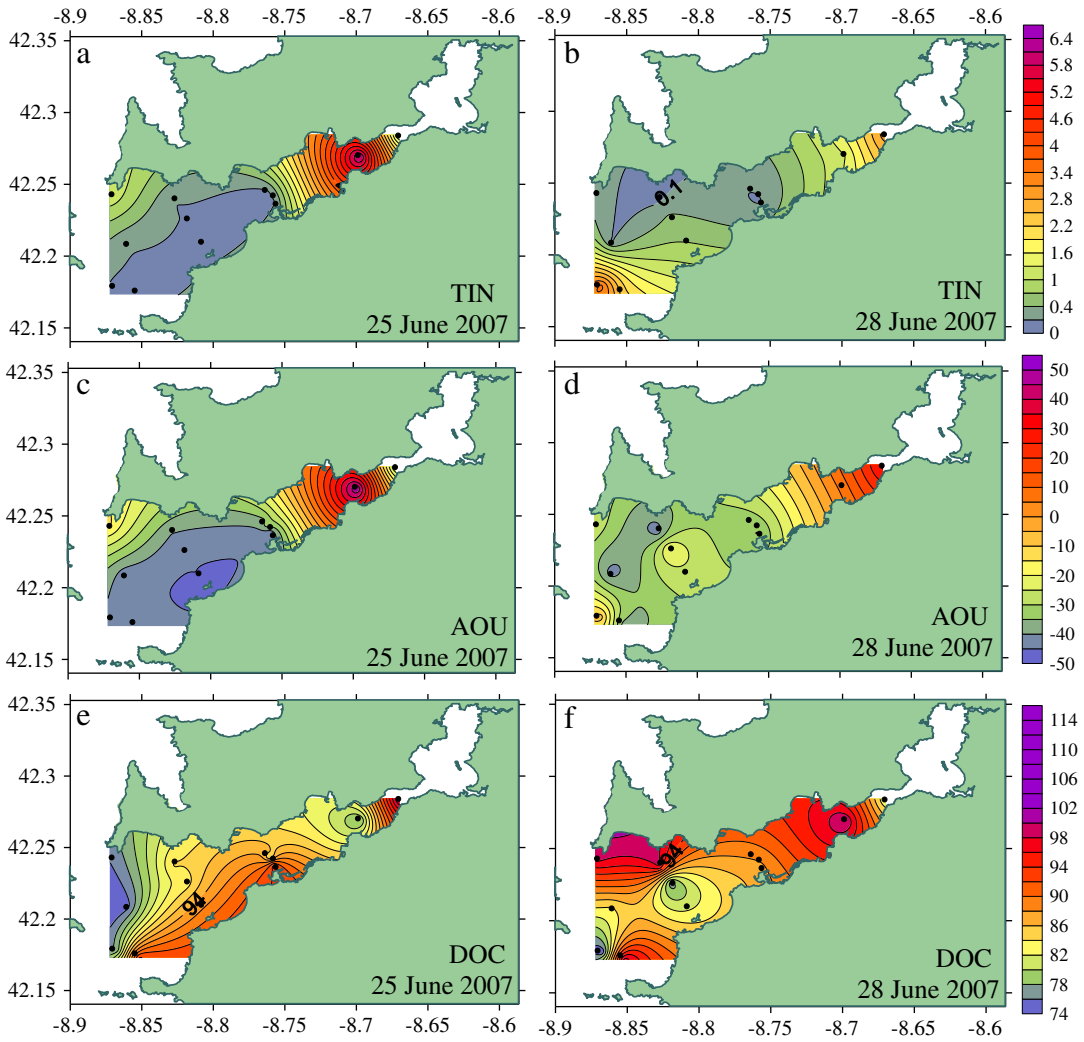

Fig. 6. Sea surface distributions for June 25 and 28 (2007) of total inorganic nitrogen (TIN) in μmol L^{-1} (a and b); apparent oxygen utilization (AOU) (c and d) in μmol kg^{-1} and of dissolved organic carbon (DOC) (e and f) in μmol L^{-1}.

other authors for coastal waters (Green and Blough, 1994; Vodacek and Blough, 1997; Ferrari et al., 1996; Ferrari, 2000; Zepp et al., 2004). The coefficients of variation of $a_{CDOM}(340)$ and $\Phi(340)$ were 26% and 14% during the downwelling and 40% and 29% during the upwelling period, respectively. Therefore, although $\Phi(340)$ was less variable than $a_{CDOM}(340)$, the variability was of the same order of magnitude. This is the reason behind the relatively low coefficients of determination found in the Ría de Vigo ($r^2 = 0.79$ for the downwelling and 0.60 for the upwelling period) compared with published values usually higher than 0.90 (Kowalczuk et al., 2010). $\Phi(\lambda)$ is altered by biotic as well as abiotic processes. On the one hand, laboratory experiments on the photobleaching of humic substances show that fluorescence decreases faster than absorption, implying a decrease of $\Phi(\lambda)$ (De Haan, 1993). On the other hand, laboratory experiment on the degradation of natural DOM from the Ría de Vigo showed that fluorescence builds up faster than absorption during the microbial production of CDOM, which implies an increase of $\Phi(\lambda)$ (Lønborg et al., 2010). Consequently, the significantly lower values of $\Phi(340)$ observed during the downwelling than during the upwelling period suggest that photodegradation was more relevant than microbial production under downwelling conditions, when the irradiated shelf surface waters entered the ría, and the contrary under upwelling conditions, when the aged ENACW upwelled on the shelf and flowed into the ría. This deduction is consistent with the significant difference observed between the regression slopes of the logarithmic plot of $a_{CDOM}(340)$ and S for both periods (see above).

4.2. Assessment of the influence of water masses mixing, microbial production and photochemical degradation on the distribution of CDOM

Concurrent absorption coefficient, induced fluorescence and DOC measurements in the coastal upwelling system of the Ría de Vigo allowed a study of the relationship among the three variables as well as the fluorescence to absorption coefficient ratios, i.e. the fluorescence quantum yield $\Phi(\lambda)$, and absorption coefficient to DOC ratio, i.e. the C-specific CDOM absorption coefficient $a^*_{CDOM}(\lambda)$. Since contrasting coastal upwelling and downwelling conditions were sampled, we have been able to characterise the optical properties of the shelf surface waters that enter the rías during downwelling events ($a_{CDOM}(340) = 0.34 \pm 0.02\ m^{-1}$, $a^*_{CDOM}(340) = 4.5 \pm 0.5\ m^2\ mol\ C^{-1}$, $\Phi(340) = 0.76 \pm 0.02\%$; average ± SD of surface samples at stn B5 in September 06) and the bottom shelf ENACW that enter the rías during upwelling events ($a_{CDOM}(340) = 0.23 \pm 0.04\ m^{-1}$, $a^*_{CDOM}(340) = 3.6 \pm 0.7\ m^2\ mol\ C^{-1}$, $\Phi(340) = 1.2 \pm 0.3\%$; average ± SD of samples colder than 14 °C in June 07). The values of $a_{CDOM}(340)$, $a^*_{CDOM}(340)$, and $\Phi(340)$ of these water types were significantly different ($p<0.001$). These two different shelf waters were forced to mix with the significantly more coloured

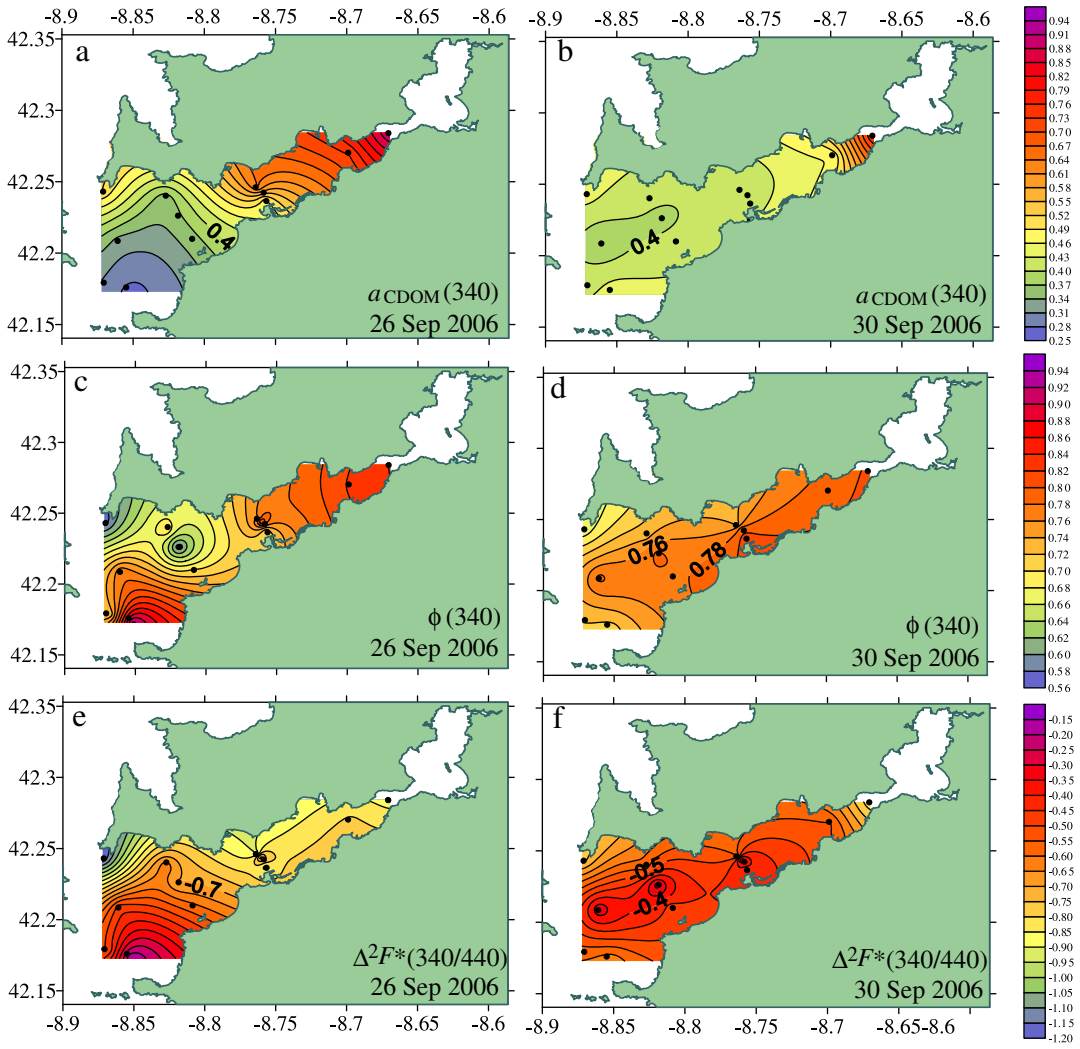

Fig. 7. Sea surface distributions for September 26 and 30 (2006) of CDOM absorption coefficient at 340 nm ($a_{CDOM}(340)$) (a and b) in m^{-1}; CDOM fluorescence quantum yield at 340 nm, $\Phi(340)$ (c and d) and $\Delta^2F^*(340/440)$ (e and f).

($a_{CDOM}(340) > 0.7\ m^{-1}$, $a^*_{CDOM}(340) > 7.5\ m^2\ mol\ C^{-1}$, $\Phi(340) > 0.8\%$) brackish waters, exported from San Simón Bay, by the positive (negative) residual circulation characteristic of upwelling-favourable (downwelling-favourable) conditions.

The distributions of the absorption coefficient and the induced fluorescence of CDOM in any marine ecosystem depend on (1) water masses mixing; and biogeochemical processes of two categories: (2) microbial and (3) photochemical. In the case of the Ría de Vigo, to remove the continental and oceanic waters mixing effects, we considered our system as a two end-member mixing problem (Doval et al., 1997; Nieto-Cid et al., 2005) that can be solved by considering the residuals of the linear correlations of the absorption coefficient and fluorescence of CDOM with salinity. Given the significant correlation of the optical properties of CDOM with DOC (Eqs. (3)–(5)), absorption coefficient and fluorescence to DOC ratios, $a^*_{CDOM}(340)$ and $F^*(340/440)$, are used to remove that dependence. During the upwelling event of June 07 the optical properties of DOM were more dependent on water mass mixing than during the downwelling event of September 06, when no significant correlations were found between either $a^*_{CDOM}(340)$ or $F^*(340/440)$ with salinity (see Eqs. 6, 7, 9 and 10 in Table 1). The residuals of the regression of $a^*_{CDOM}(340)$ with salinity, $\Delta a^*_{CDOM}(340)$, correlated significantly with the residuals of the correlation of $F^*(340/440)$ with salinity, $\Delta F^*(340/440)$, (see Eq. 12 in Table 1) and the slope of that correlation, 4.8 ± 0.4 m QSU, was not significantly different for both study periods. If this slope of 4.8 ± 0.4 m QSU is multiplied by the conversion factor $2.2\ (\pm 0.2)\ 10^{-3}\ m^{-1}\ QSU^{-1}$ of Eq. (5) produces a value of $1.1 \pm 0.1\%$ that can be considered the average $\Phi(340)$ of the Ría de Vigo, independently of the mixing of water masses and the dominant hydrographic conditions. However, the linear correlation between $\Delta F^*(340/440)$ and $\Delta a^*_{CDOM}(340)$ explains only 46% of the observed variability ($R^2 = 0.46$ form Eq. 12 in Table 1). Figs. 7e and f and 8e and f show the horizontal distributions of the residuals of the linear regression between $\Delta F^*(340/440)$ and $\Delta a^*_{CDOM}(340)$, $\Delta^2F^*(340/440)$. The variability of $\Delta^2F^*(340/440)$ is equivalent to the variability of $\Phi(340)$ independent of the mixing of water masses. If the distributions of $\Delta^2F^*(340/440)$ were stochastic it would mean that the values of $\Delta^2F^*(340/440)$ are just a consequence of the errors associated to the collection and determination of $F^*(340/440)$ and $a^*_{CDOM}(340)$. However, the distributions of $\Delta^2F^*(340/440)$ are systematic: the values are predominantly negative in September 06 (Fig. 7e and f) and predominantly positive in June 07 (Fig. 8e and f). For a given period, they increase down- and shore-wards. A systematic distribution of residuals means that environmental factors, other than the mixing of water masses, are affecting the distributions of $F^*(340/440)$ and $a^*_{CDOM}(340)$.

Considering that $\Phi(340)$ decreases during photo-degradation (De Haan, 1993) and increases during microbial degradation (Lønborg et al., 2010) processes, and that the variability of $\Delta^2F^*(340/440)$ is equivalent to the variability of $\Phi(340)$, positive values of $\Delta^2F^*(340/440)$ indicate a larger relative influence of microbial degradation

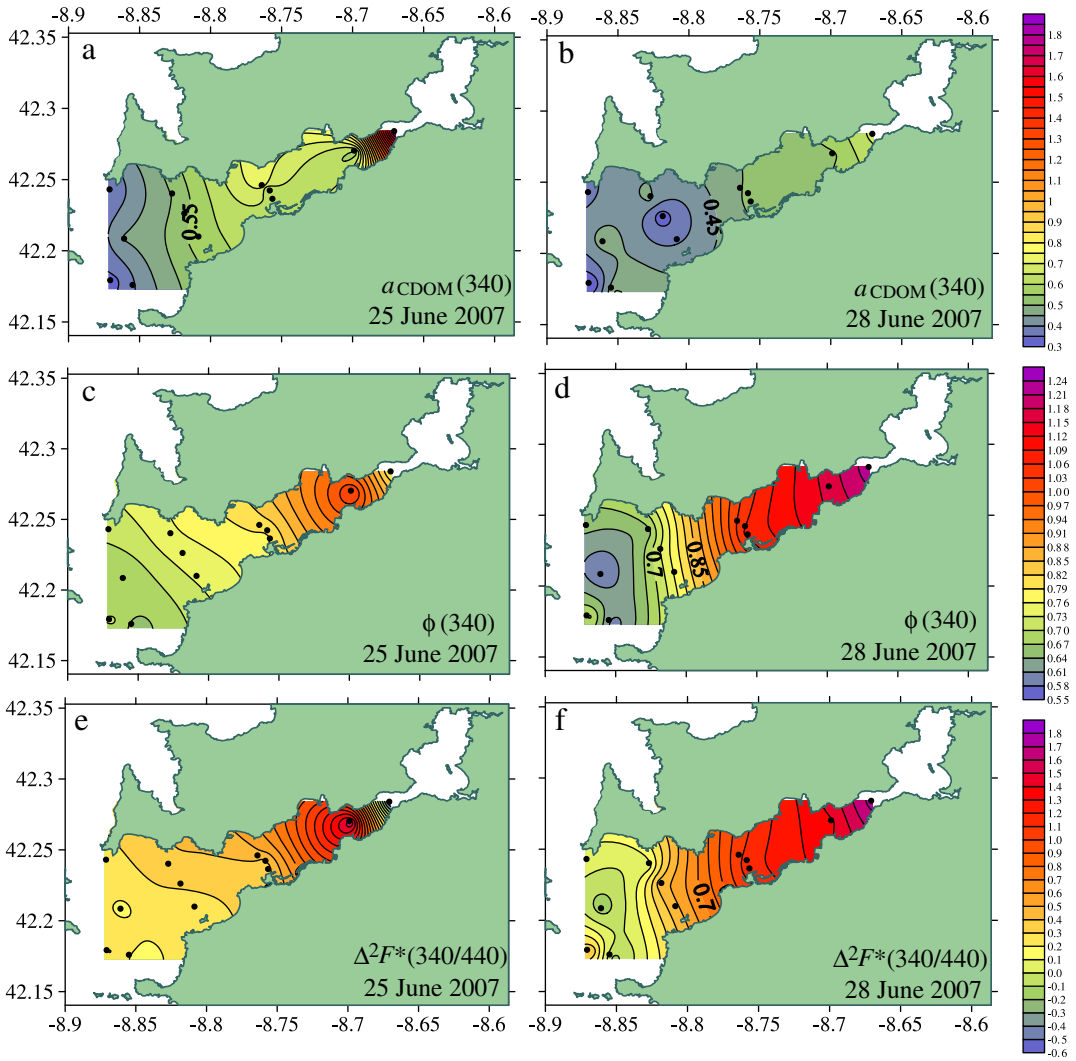

Fig. 8. Sea surface distributions for June 25 and 28 (2007) of CDOM absorption coefficient at 340 nm ($a_{CDOM}(340)$) (a and b) in m^{-1}; CDOM fluorescence quantum yield at 340 nm, Φ (340) (c and d) and $\Delta^2F^*(340/440)$ (e and f).

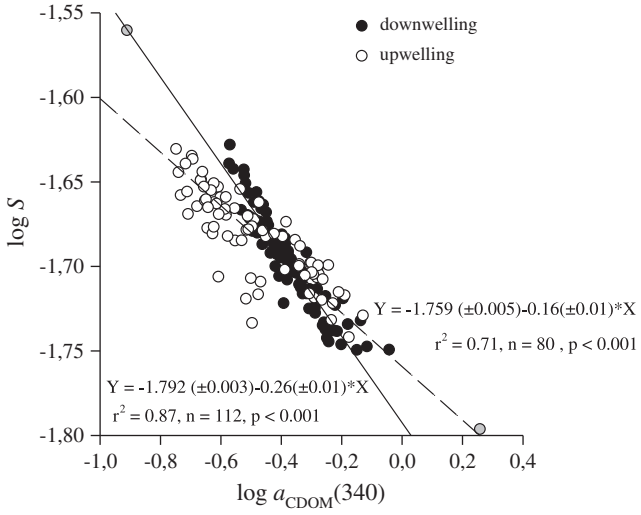

Fig. 9. Logarithmic plot of the spectral slope, S in the range of 250–500 nm versus absorption coefficient at 340 nm, $a_{CDOM}(340)$, for the downwelling (black dots) and upwelling period (open dots).

processes while negative values a larger relative influence of photo degradation processes. Consequently, microbial processes were more relevant in June 07 than in September 06 and within each period, photochemical processes gained importance in the surface layer of the outermost stations.

The relative importance of photochemical and microbial respiration processes on the distributions of $\Delta F^*(340/440)$ and $\Delta a^*_{CDOM}(340)$ can be quantified by means of the parameters of the multiple linear regression of $\Delta F^*(340/440)$ versus ΔAOU and $\Delta a^*_{CDOM}(340)$ for

Table 2
Average ± SD values of the absorption coefficient (m^{-1}) at several wavelengths, the spectral slope over the 250–500 nm wavelength range, and the fluorescent quantum yield at 340 nm for downwelling, upwelling, and both period in the Ría de Vigo. All samples collected in September 06 and June 07 were used to calculate the average ± SD values for downwelling and upwelling conditions, respectively. The last column of Table 2 was produced with all the samples collected in both periods.

	Downwelling	Upwelling	Downwelling + upwelling
$a_{CDOM}(325)$	0.57 ± 0.03	0.47 ± 0.19	0.54 ± 0.17
$a_{CDOM}(340)$	0.43 ± 0.11	0.35 ± 0.14	0.40 ± 0.13
$a_{CDOM}(355)$	0.32 ± 0.08	0.26 ± 0.11	0.29 ± 0.10
$a_{CDOM}(375)$	0.21 ± 0.06	0.17 ± 0.08	0.20 ± 0.07
$a_{CDOM}(443)$	0.055 ± 0.02	0.043 ± 0.02	0.051 ± 0.023
S	0.020 ± 0.001	0.02 ± 0.001	0.021 ± 0.001
$\Phi(340)$	0.81 ± 0.11%	1.03 ± 0.30%	0.91 ± 0.3

each period (Eqs. 13 and 14 in Table 1). The AOU reflects the net ecosystem metabolism (NEM; Smith and Hollibaugh, 1997), this is the net production of dissolved oxygen due to primary producers minus the net consumption by the respiration of all the autotrophs and heterotrophs living in the study system. Previous studies in the Ría de Vigo have demonstrated that the oxygen budget of this embayment is controlled by the microbial food web (Cermeño et al., 2006; Piedracoba et al., 2008). In addition, the AOU in the surface mixed layer is affected by the exchange of dissolved oxygen with the atmosphere when moderate to strong winds blow into the ría (Piedracoba et al., 2008). For the particular case of the study period, the average ± SD local wind speed estimated at 10 m over the sea surface (u_{10}) was 0.79 ± 0.78 m s^{-1} in September 06 and 1.66 ± 0.82 m s^{-1} in June 07. The corresponding piston velocities (k) calculated with the Wanninkhof's (1992) formula, $k = 0.31\, u_{10}^2 \cdot (Sc/589)^{-1/2}$, were 0.04 and 0.20 m d^{-1}, respectively. Sc is the dimensionless Schmidt number. With these values of k, the average AOU of the surface layer (−41 ± 20 μmol kg^{-1} for September 06 and −25 ± 25 μmol kg^{-1} for June 07) and considering that the surface layer is 5 m thick, the resulting oxygen fluxes would be as low as 0.36 μmol kg^{-1} d^{-1} in September 06 and 0.97 μmol kg^{-1} d^{-1} in June 07, in both cases from the sea surface to the atmosphere. Given that the flushing time of the surface layer during moderate upwelling and downwelling events in the Ría de Vigo is about 2–3 days (Álvarez-Salgado et al., 2001; Piedracoba et al., 2008), oxygen exchange can be neglected for the purposes of this work. Therefore, AOU is an unequivocal indicator of the aerobic microbial metabolism and ΔAOU are the residuals of the linear regression of AOU with salinity, which is significant during the downwelling event of September 06 and the upwelling event of June 07 (Eqs. 8 and 11 in Table 1).

When the variables $\Delta F^*(340/440)$, ΔAOU and $\Delta a^*_{CDOM}(340)$ are normalised and the regression slopes are of the same sign, the square of the resulting normalised regression slope (β_1^2) indicates the proportion of the variability of $\Delta F^*(340/440)$ explained by ΔAOU if $\Delta a^*_{CDOM}(340)$ is kept constant. Consistently, β_2^2 indicates the proportion of the variability of $\Delta F^*(340/440)$ explained by $\Delta a^*_{CDOM}(340)$ if ΔAOU is kept constant. Therefore, the ratio $\beta_1^2/(\beta_1^2+\beta_2^2)$ indicates the proportion of the biogeochemical variability of $\Delta F^*(340/440)$ that is due to microbial respiration and $\beta_2^2/(\beta_1^2+\beta_2^2)$ the proportion due to photo degradation. Eqs. (13) and (14) in Table 1 show the values of β_1 and β_2. For the downwelling period of September 2006, $\beta_1 = 0.27 \pm 0.07$ and $\beta_2 = 0.66 \pm 0.07$. Therefore, the relative contribution of photo- and biodegradation processes would be 86% and 14%, respectively. If the same procedure is followed for the upwelling event of June 07, only 23% of the variability of $\Delta F^*(340/440)$ was due to photochemical process while 77% was due to microbial respiration. Note that $R^2 > \beta_1^2+\beta_2^2$ in both periods because the two predictor variables, $\Delta a^*_{CDOM}(340)$ and ΔAOU, covaried between themselves. However, using β_1 and β_2 ensures that the dependence of the predictor variables among them is ruled out of the analysis. Therefore, in this section we have been able to quantify the differential impact of microbial and photochemical processes on the optical properties of CDOM under contrasting downwelling and upwelling conditions. These differences had been previously suggested qualitatively by the distributions of $\Phi(340)$ and the regression slopes of the logarithmic plot of $a_{CDOM}(340)$ and S for both periods.

5. Conclusions

Absorption coefficient and induced fluorescence of CDOM have been recurrently used in the literature to estimate DOC concentrations in coastal systems. The success of the prediction of DOC from $a_{CDOM}(\lambda)$ and/or $F(\lambda)$ depends on a narrow variability of the carbon specific CDOM absorption coefficient, $a^*_{CDOM}(\lambda)$, and the fluorescence quantum yield, $\Phi(\lambda)$. The best estimates have been obtained in coastal areas affected by strong freshwater influences, where the variability of $a^*_{CDOM}(\lambda)$ and $\Phi(\lambda)$ is usually several orders of magnitude lower than $a_{CDOM}(\lambda)$ and $F(\lambda)$. However, our work shows that a detailed study of the limited spatial and temporal variability of $\Phi(\lambda)$ in a particular coastal system can help to elucidate the relative importance of the microbial and photochemical processes that control the changes of the absorption coefficient and induced fluorescence properties produced and consumed in that system. In the case study of the Ría de Vigo, we obtained that 86% of the variability of $\Phi(340)$ during the mixing of shelf surface and continental waters under downwelling conditions was due to the photodegradation of CDOM. On the contrary, during the mixing of bottom shelf and continental waters under upwelling conditions, 77% of the variability of $\Phi(340)$ was due to microbial respiration. Concurrent induced fluorescence and absorption coefficient measurements in other coastal system would allow application of this methodology to infer the biogeochemical processes that control CDOM variability during estuarine mixing.

Acknowledgements

We wish to express our gratitude to all the participants in the CRIA project and to the captain and crew of the R/V Mytilus. Support for this work came from the Xunta de Galicia, grant number PGIDIT-05MA40201PR. C.M. was funded by project SUMMER, grant number CTM2008-03309/MAR, C.R.-C. was funded by a I3P-CSIC predoctoral fellowship and N.N.-C. was funded by a Marie Curie I.O.F. to carry out this work. We wish also express our gratitude to two anonymous reviewers for their comments.

References

Álvarez-Salgado, X.A., Rosón, G., Pérez, F.F., Pazos, Y., 1993. Hydrographic variability off the Rías Baixas (NW Spain) during the upwelling season. J. Geophys. Res. 98, 14447–14455 Hydrographic Variability off the Rías Baixas (NW Spain) During the Upwelling Season.

Álvarez-Salgado, X.A., Gago, J., Miguez, B.M., Perez, F.F., 2001. Net ecosystem production of dissolved organic carbon in a coastal upwelling system: the Ria de Vigo, Iberian Margin of the North Atlantic. Limnol. Oceanogr. 46, 135–147.

Babin, M., Stramski, D., Ferrari, G.M., Claustre, H., Bricaud, A., Obolensky, G., Hoepffner, N., 2003. Variations in the light absorption coefficients of phytoplankton, nonalgal particles, and dissolved organic matter in coastal waters around Europe. J. Geophys. Res. 108, 3122.

Blough, N.V., Del Vecchio, R., 2002. Chromophoric dissolved organic matter (CDOM) in the coastal environment. In: Hansell, D., Carlson, C. (Eds.), 2002. Biogeochemistry of Marine Dissolved Organic Matter. Academic Press, San Diego, pp. 509–546.

Bricaud, A., Morel, A., Prieur, L., 1981. Absorption by dissolved organic matter of the sea (yellow substance) in the UV and visible domains. Limnol. Oceanogr. 26, 43–53.

Cermeño, P., Marañón, E., Pérez, V., Serret, P., Fernández, E., Castro, C.G., 2006. Phytoplankton size structure and primary production in a highly dynamic coastal ecosystem (Ría de Vigo, NW-Spain): seasonal and short-time scale variability. Estuar. Coast. Shelf Sci. 67, 251–266.

Chen, R.F., Bada, J.L., 1992. The fluorescence of dissolved organic matter in seawater. Mar. Chem. 37, 191–221.

Chen, R.F., Zhang, Y., Vlahos, P., Rudnick, S.M., 2002. The fluorescence of dissolved organic matter in the Mid-Atlantic Bight. Deep Sea Res. II 49 (20), 4439–4459.

Coble, P.G., 1996. Characterization of marine and terrestrial DOM in seawater using excitation-emission matrix spectroscopy. Mar. Chem. 51, 325–346.

Coble, P.G., 2007. Marine optical biogeochemistry: the chemistry of ocean color. Chem. Rev. 107, 402–418.

Coble, P.G., Del Castillo, C.E., Avril, B., 1998. Distribution and optical properties of CDOM in the Arabian Sea during the 1995 Southwest Monsoon. Deep Sea Res. II 45, 2195–2223.

Day, D.A., Faloona, I., 2009. Carbon monoxide and chromophoric dissolved organic matter cycles in the shelf waters of the northern California upwelling system. J. Geophys. Res. 114, C01006.

De Haan, H., 1993. Solar UV-light penetration and photodegradation of humic substances in peaty lake water. Limnol. Oceanogr. 38, 1072–1076.

Del Castillo, C.E., Coble, P.G., 2000. Seasonal variability of the colored dissolved organic matter during the 1994–95 NE and SW monsoons in the Arabian Sea. Deep Sea Res. II 47, 1563–1579.

Del Castillo, C.E., Miller, R.L., 2008. On the use of ocean color remote sensing to measure the transport of dissolved organic carbon by the Mississippi River Plume. Remote Sens. Environ. 112, 836–844.

Del Vecchio, R., Blough, N.V., 2004. Spatial and seasonal distribution of chromophoric dissolved organic matter and dissolved organic carbon in the Middle Atlantic Bight. Mar. Chem. 89, 169–187.
Doval, M.D., Álvarez-Salgado, X.A., Fiz, F.P.R., 1997. Dissolved organic matter in a temperate embayment affected by coastal upwelling. Mar. Ecol. Prog. Ser. 157, 21–37.
Eppley, R.W., Peterson, B.J., 1979. Particulate organic matter flux and planktonic new production in the deep ocean. Nature 282, 677–680.
Ferrari, G.M., 2000. The relationship between chromophoric dissolved organic matter and dissolved organic carbon in the European Atlantic coastal area and in the West Mediterranean Sea (Gulf of Lions). Mar. Chem. 70, 339–357.
Ferrari, G.M., Dowell, M.D., Grossi, S., Targa, C., 1996. Relationship between the optical properties of chromophoric dissolved organic matter and total concentration of dissolved organic carbon in the southern Baltic Sea region. Mar. Chem. 55, 299–316.
Figueiras, F.G., Ríos, A.F., 1993. Phytoplankton succession, red tides and the hydrographic regime in the Rias Bajas of Galicia. In: Smayda, T.J., Shimizu, Y. (Eds.), Toxic Phytoplankton Blooms in the Sea. Elsevier Science Publishers B.V, pp. 239–244.
Gago, J., Álvarez-Salgado, X.A., Nieto-Cid, M., Brea, S., Piedracoba, S., 2005. Continental inputs of C, N, P and Si species to the Ría de Vigo (NW Spain). Estuar. Coast. Shelf Sci. 65, 74–82.
Green, S.A., Blough, N.V., 1994. Optical absorption and fluorescence properties of chromophoric dissolved organic matter in natural waters. Limnol. Oceanogr. 39, 1903–1916.
Häder, D.-P., Sinha, R.P., 2005. Solar ultraviolet radiation-induced DNA damage in aquatic organisms: potential environmental impact. Mutat. Res. 571, 221–233.
Hoge, F.E., Swift, R.N., Yungel, J.K., 1993. Fluorescence of dissolved organic matter: a comparison of North Pacific and North Atlantic Oceans during April 1991. J. Geophys. Res. 98, 22,779–22,787.
Kieber, R.J., Hydro, L.H., Seaton, P.J., 1997. Photooxidation of triglycerides and fatty acids in seawater: implication toward the formation of marine humic substances. Limnol. Oceanogr. 42, 1454–1462.
Klinkhammer, G.P., McManus, J., Colbert, D., Rudnicki, M.D., 2000. Behavior of terrestrial dissolved organic matter at the continent-ocean boundary from high-resolution distributions. Geochim. Cosmochim. Acta 64, 2765–2774.
Kowalczuk, P., Cooper, W.J., Durako, M.J., Kahn, A.E., Gonsior, M., Young, H., 2010. Characterization of dissolved organic matter fluorescence in the South Atlantic Bight with use of PARAFAC model: relationships between fluorescence and its components, absorption coefficients and organic carbon concentrations. Mar. Chem. 118, 22–36.
Kramer, G.D., Herndl, G.J., 2004. Photo- and bioreactivity of chromophoric dissolved organic matter produced by marine bacterioplankton. Aquat. Microb. Ecol. 36, 239–246.
Kudela, R.M., Garfield, N., Brulanda, K.W., 2006. Bio-optical signatures and biogeochemistry from intense upwelling and relaxation in coastal California. Deep Sea Res. II 53, 2999–3022.
Lønborg, C., Alvarez-Salgado, X.A., Martinez-Garcia, S., Miller, A.E.J., Teira, E., 2010. Stoichiometry of dissolved organic matter and the kinetics of its microbial degradation in a coastal upwelling system. Aquat. Microb. Ecol. 58, 117–126.
Melhuish, W.H., 1961. Quantum efficiencies of fluorescence of organic substances: effect of solvent and concentration of the fluorescent solute. J. Phys. Chem. 65, 229–235.
Moran, M.A., Sheldon, W.M., Zepp, R.G., 2000. Carbon loss and optical property changes during long-term photochemical and biological degradation of estuarine dissolved organic matter. Limnol. Oceanogr. 45, 1254–1264.
Nelson, N.B., Craig, A.C., Steinberg, D.K., 2004. Production of chromophoric dissolved organic matter by Sargasso Sea microbes. Mar. Chem. 89, 273–287.
Nelson, N.B., Siegel, D.A., Carlson, C.A., Swan, C., Smethie Jr., W.M., Khatiwala, S., 2007. Hydrography of chromophoric dissolved organic matter in the North Atlantic. Deep Sea Res. I 54, 710–731.
Nelson, N.B., Siegel, D.A., Carlson, C.A., Swan, C.M., 2010. Tracing global biogeochemical cycles and meridional overturning circulation using chromophoric dissolved organic matter. Geophys. Res. Lett. 37, L03610.
Nieto-Cid, M., Álvarez-Salgado, X.A., Gago, J., Pérez, F.F., 2005. DOM fluorescence, a tracer for biogeochemical processes in a coastal upwelling system (NW Iberian Peninsula). Mar. Ecol. Prog. Ser. 297, 33–50.
Nieto-Cid, M., Álvarez-Salgado, X.A., Pérez, F.F., 2006. Microbial and photochemical reactivity of fluorescent dissolved organic matter in a coastal upwelling system. Limnol. Oceanogr. 51, 1391–1400.
Piedracoba, S., Nieto-Cid, M., Teixeira, I.G., Garrido, J.L., Álvarez–Salgado, X.A., Rosón, G., Castro, C.G., Pérez, F.F., 2008. Physical–biological coupling in the coastal upwelling system of the Ría de Vigo (NW Spain). II: an in vitro approach. Mar. Ecol. Progr. Ser. 353, 41–53.
Romera-Castillo, C., Sarmento, H., Álvarez-Salgado, A.X., Gasol, J.M., Marrasé, C., 2010. Production of chromophoric dissolved organic matter by marine phytoplankton. Limnol. Oceanogr. 55, 446–454.
Siegel, D.A., Maritorena, S., Nelson, N.B., 2002. Global distribution and dynamics of colored dissolved and detrital organic materials. J. Geophys. Res. 107, 3228.
Smith, S.V., Hollibaugh, J.T., 1997. Annual cycle and interannual variability of ecosystem metabolism in a temperate climate embayment. Ecol. Monogr. 67, 509–533.
Sokal, F.F., Rohlf, F.J., 1995. Biometry. Freeman.
Stedmon, C.A., Markager, S., 2001. The optics of chromophoric dissolved organic matter (CDOM) in the Greenland Sea: an algorithm for differentiation between marine and terrestrially derived organic matter. Limnol. Oceanogr. 46, 2087–2093.
Stedmon, C.A., Markager, S., Kaas, H., 2000. Optical properties and signatures of Chromophoric Dissolved Organic Matter (CDOM) in Danish coastal waters. Estuar. Coast. Shelf Sci. 51, 267–278.
Stedmon, C.A., Osburn, C.L., Kragh, T., 2010. Tracing water mass mixing in the Baltic–North Sea transition zone using the optical properties of coloured dissolved organic matter. Estuar. Coast. Shelf Sci. 87, 156–162.
Swan, C.M., Siegel, D.A., Nelson, N.B., Carlson, C.A., Nasir, E., 2009. Biogeochemical and hydrographic controls on chromophoric dissolved organic matter distribution in the Pacific Ocean. Deep Sea Res. I 56, 2175–2192.
Torres, R., Barton, E.D., Miller, P., Fanjul, E., 2003. Spatial patterns of wind and sea surface temperature in the Galician upwelling region. J. Geophys. Res. 108, 3130.
Vodacek, A., Blough, N.V., 1997. Seasonal variation of CDOM and DOC in the Middle Atlantic Bight: terrestrial inputs and photooxidation. Limnol. Oceanogr. 42, 674–686.
Vodacek, A., Hoge, F.E., Swift, R.N., Yungel, J.K., Peltzer, E.T., Blough, N.V., 1995. The use of in situ and airborne fluorescence measurements to determine UV absorption coefficients and DOC concentrations in surface waters. Limnol. Oceanogr. 40, 411–415.
Wanninkhof, R., 1992. Relationship between wind speed and gas exchange over the ocean. J. Geophys. Res. 97, 7373–7382.
Wooster, W.S., Bakun, A., McLain, D.R., 1976. The seasonal upwelling cycle along the eastern boundary of the North Atlantic. J. Mar. Res. 34, 131–140.
Yamashita, Y., Tanoue, E., 2008. Production of bio-refractory fluorescent dissolved organic matter in the ocean interior. Nat. Geosci. 1, 579–582.
Yentsch, C.S., Reichert, C.A., 1961. The interrelationship between water-soluble yellow substances and chloroplastic pigments in marine algae. Bot. Mar. 3, 65–74.
Zepp, R.G., Sheldon, W.M., Moran, M.A., 2004. Dissolved organic fluorophores in southeastern US coastal waters: correction method for eliminating Rayleigh and Raman scattering peaks in excitation–emission matrices. Mar. Chem. 89, 15–36.

Glossary

$a_{CDOM}(\lambda)$: Absorption coefficient at wavelength λ
$a^*_{CDOM}(340)$: Carbon specific CDOM absorption coefficient at 340 nm
AOU: Apparent oxygen utilization
CDOM: Coloured dissolved organic matter
ENACW: Eastern North Atlantic Central Water
FDOM: Fluorescent dissolved organic matter
F(340/440): FDOM at Ex/Em 340 nm/440 nm
QSU: Quinine sulphate units
S: Spectral slope
s: Salinity
TIN: Total inorganic nitrogen
$\Delta a^*_{CDOM}(340)$: Residual of $a^*_{CDOM}(340)$ with salinity
ΔAOU: Residual of AOU with salinity
$\Delta F^*(340/440)$: Residual of C-specific fluorescence with salinity
$\Delta^2 F^*(340/440)$: Residual of $\Delta F^*(340/440)$ versus $\Delta a^*_{CDOM}(340)$
$\Phi(340)$: Fluorescent quantum yield at 340 nm